*metals*

MDPI

*Article*

# Niobium's Effect on the Properties of a Quasi-High-Entropy Alloy of the CoCrFeMnNi System

**Svetlana Kvon, Aristotel Issagulov, Vitaliy Kulikov and Saniya Arinova ***

Department of Nanotechnology and Metallurgy, Karaganda Technical University, Nazarbayev Avenue No. 56, Karaganda 100027, Kazakhstan; svetlana.1311@mail.ru (S.K.); aristotel_isagulov@mail.ru (A.I.); mlpikm@mail.ru (V.K.)

* Correspondence: sanya_kazah@mail.ru; Tel.: +7-2-1256-7841

**Abstract:** This paper deals with the possibility of smelting quasi-high-entropy alloys (QHEAs) with the partial use of ferroalloys in the charge instead of pure metals. The Cantor alloy (CoCrFeMnNi) was used as the base alloy and the comparison sample, into which niobium was introduced in the amount of 14 to 18% by weight. The structure, hardness, strength, and tribological properties of prototypes were studied. The results obtained showed, on the one hand, the possibility of using ferroalloys as charge components in the smelting of QHEAs and, on the other hand, the positive effect of niobium in the amount of 14–17% on the strength and wear resistance of the alloy. Increasing the niobium content above 18% leads to its uneven distribution in the structure, consequently decreasing the strength and wear resistance of the alloy. The structure of the studied alloys is represented by a solid solution of FCC, which includes all metals, and the niobium content varies widely. In addition, the structure is represented by the phases of implementation: niobium carbide NbC 0.76–1.0, manganese carbide $Mn_7C_3$, and a CrNi intermetallic compound with a cubic lattice.

**Keywords:** quasi-high-entropy alloy (QHEA); ferroalloy; ferroniobium; strength; wear resistance; fluidity

**Citation:** Kvon, S.; Issagulov, A.; Kulikov, V.; Arinova, S. Niobium's Effect on the Properties of a Quasi-High-Entropy Alloy of the CoCrFeMnNi System. *Metals* **2024**, *14*, 564. https://doi.org/10.3390/met14050564

Academic Editor: Jiro Kitagawa

Received: 5 April 2024
Revised: 28 April 2024
Accepted: 3 May 2024
Published: 10 May 2024



## 1. Introduction

High-entropy alloys are popular objects of research because they demonstrate superior performance properties compared to traditional steels and other alloys used for similar purposes [1–7]. The fundamental difference between high-entropy alloys and classical alloys lies in the approach to their development. In HEAs, there is no main base element, such as iron in steels. In HEAs, all components play approximately equal roles in the formation of the structure and properties. This difference is clearly illustrated by the diagram shown in Figure 1 [3].

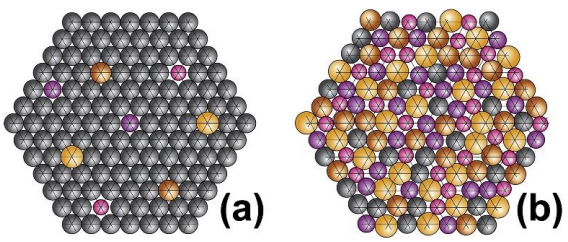


**Figure 1.** Illustration of the atom distribution in a "classical" alloy (**a**) and in an HEA (**b**) (data from Ref. [1]).

Later, more complex systems began to be attributed to wind farms, in which strict equiatomic concentration was no longer observed, but the basic principle of creating

wind farms—the absence of a dominant element—remained [8–12]. The structure of such alloys is more complex; in addition to the solid solution, the presence of other phases is observed: Laves phases, intermetallic compounds, mixtures of solid solutions of various types, etc. Taking into account this trend, the creation of WPPs can already be considered as the next step in the development of complex alloy steels, such as heat- and corrosion-resistant steels [13].

It should be noted that WPPs based on transition metals are the most widespread and, accordingly, the most studied. The first wind turbines based on the CoCrFeNiMn system were studied in [1]; the CoCrFeNiMn alloy in equiatomic concentration is a classic (Cantor) alloy.

The research of this alloy was then further developed. Various elements were added to the system, mainly IV and V groups of the periodic table, such as Mo, Ti, V, and Nb, as well as Cu, Al, C, etc. [12,14–18]. The introduction of these elements into the composition of alloys leads to an increase in hardness, strength, corrosion resistance, and a number of other properties.

Works [19–24] are devoted to the study of the effect of niobium on the properties of alloys of the CoCrFeNiMn system. Niobium has a large atomic radius of 145 nm; for comparison, the atomic radius of iron is 0.126 nm, and niobium is therefore often used as an element for solid solution hardening. In all of these works, the positive effect of niobium on the strength properties of the alloy is noted. In studies [20,21], it was shown that the structure of alloys based on the CoCrFeNiMnNb system is represented by eutectic consisting of a solid solution, which includes all elements and a Laves phase, which actually plays the role of a strengthening phase in these alloys.

At the same time, it should be noted that, despite the expansion of WPP compositions and the variety of structures, all of the studied WPPs have one common feature. Wind turbines are smelted from high-purity metals, and rather complex smelting technologies are used to produce them, including multiple remelting, a protective medium or vacuum, and plasma synthesis. Accordingly, these smelting conditions and strict requirements for the charge significantly increase the cost of wind farms, which reduces their commercial attractiveness and direct use in production.

The object of this study are alloys of the CoCrFeNiMnNb system, fused with the partial use of ferroalloys in the charge. This makes it possible to simplify the smelting technology by reducing the melting point of the charge materials and increasing the commercial attractiveness of the final product.

It should be noted that ferroalloys are not two-component systems. In addition to iron and other relevant metals (Mn, Cr, Nb, etc.), they also contain impurities such as C, Si, S, and P. It is obvious that the presence of impurities in the composition of the charge will have a significant impact on the formation of the structure and phase composition of the alloy.

The purpose of this study is to determine the possibility of smelting WPPs based on the CoCrFeNiMnNb system with the partial replacement of pure metals in the charge with appropriate ferroalloys, and to investigate the properties and structure of the obtained alloys.

Due to the fact that not only pure metals, but corresponding ferroalloys, will be used for the smelting of experimental alloys in this study, as well as simpler smelting conditions, it is more appropriate to call the obtained experimental alloys quasi-high-entropy (CES) in the context of pseudo-high-entropy. Such terminology has already been used in other works [17,25].

## 2. Materials and Methods

Ferromanganese of the FeMn80C05 grade, ferrochrome of the FCh001A grade, ferroniobium of the FNb58 grade, metallic nickel of the N-1u grade, and metallic cobalt of the K1Au grade were used as charge materials. The composition of the charge was selected in such a way that the Nb content in the final alloy varied from 14 to 18%; the

content of each of the other elements would average about 16.5%. It is in this ratio of the composition of the alloy that the composition will be close to an equiatomic one. The chemical composition of the charge materials is given in Table 1.

**Table 1.** The charge composition.

| Material / Element, % | FeMn80C05 | FCh001A | FNb58 | Ni N-1u | Co K1Au |
|---|---|---|---|---|---|
| Mn | 75.1 | - | - | - | 0.03 |
| Nb | - | - | 62 | - | - |
| Fe | 25.2 | 32.04 | 35.5 | - | 0.2 |
| Cr | - | 68.2 | - | - | - |
| Ni | - | - | - | 99.95 | - |
| Co | - | - | - | - | 99.3 |
| C | up to 0.1 | up to 0.1 | 0.3 | up to 0.1 | 0.02 |
| Si | 1.85 | 0.82 | 1.8 | 0.002 | - |
| P | up to 0.3 | up to 0.02 | 0.04 | 0.001 | 0.003 |
| S | up to 0.03 | up to 0.02 | 0.05 | 0.001 | 0.004 |

The dispersion of all of the components was 90% represented by the fraction of 2–3 mm. The fractional composition of the materials was determined on an analytical sieving machine AS 200 control (Retsch, Haan, Germany). Next, the charge mixture was thoroughly mixed within 15 min in a Schatz laboratory mixer and melted in a UIP-16 induction furnace with an enhanced cooling system in an air atmosphere. Melting was carried out in a graphite crucible. Next, the resulting melt (approximate weight 0.4 kg) at the temperature of 1680 °C was poured into corundum–mullite–zirconium (CMC) crucibles, cooled, and remelted, and again poured into the CMC crucible. Remelting was carried out to homogenize the structure and to eliminate segregation throughout the body of the ingot. After complete cooling, samples for analysis were prepared using the ingot. The chemical composition, hardness, compressive strength, structure, and tribological properties were studied on prototypes.

The chemical composition was determined using a Poly Spec-F spectrometer (ITPhotonics S.r.l., Fara Vicentino, Italia)

Tribological tests of samples were carried out on a Tribometer set (the CSM Instruments, Peseux, Switzerland) using the measuring slide method under the following conditions: track length, 4 mm; applied load, 1 N; speed, 5 cm/s; counterbody, ball with a diameter of 3 mm made of WC-Co (VK6); mileage, 20,000 cycles (160 m); medium, air; pretreatment of samples, ultrasonic cleaning (USC) in isopropyl alcohol.

These tests comply with the ASTM G99-05(2010) [26], ASTM G133-05(2010) [27], and DIN50324 [28] international standards and are used to evaluate the wear resistance of materials. The coefficient of friction of a rubbing pair is equal to the ratio of the measured friction force to the pressing force. The reduced wear resistance was assessed based on the parameters of the wear groove on the sample and the wear scar on the counterbody according to the formula:

$$\varepsilon' = \frac{W}{A}$$

where $W$ is the wear debris volume, $mm^3$; $A$ is the friction work, N*m.

The parameters of the wear grooves to determine the volume of wear debris were determined on a WYKO NT1100 optical profilometer (Veeco Instruments Inc, Plainview, NY, USA). The results of the tribological tests were automatically processed using Instrum X for Tribometer, CSM instruments.

Hardness was determined using a Willson 1150 device (Willson, Lake Bluff, Illinois, USA), with measurements carried out at at least 5 points.

The compressive strength was determined on an INSTRON testing machine, Buckinghamshire, England with 3 takes. The ductility was not determined. Relative unit shortening was defined as a characteristic of plasticity. The test samples had a cylindrical shape of 10 × 15 mm². The load application speed was 5 mm/min, the test temperature was 25 °C, and the accuracy of the displacement measurement was ±0.05%.

The conditional compressive strength was determined using the formula

$$\sigma_b = \frac{P}{F_0},$$

where $P$ is the maximum load on the sample, N; and $F_0$ is the initial cross-sectional area of the sample, m².

The unit shortening $\varepsilon$ was determined by the formula

$$\varepsilon_l = \frac{l_0 - l_к}{l_0},$$

where $l_к$ is the final length of the sample, mm; and $l_0$ is the initial length of the sample, mm.

The structure was analyzed using a scanning electron microscope (S-3400N) equipped with a NORAN X-ray energy-dispersive spectrometer from the Hitachi High Technologies Corporation (Tokyo, Japan); the resolution of the microscope in deep vacuum mode was 3–4 nm.

Graphical studies were carried out on the X'expert Pro diffractometer using CuKa radiation (Panalytical, Almelo, Netherlands). The maximum voltage was 30 kV, the current was 10 mA, and a nickel filter was used. The diffraction spectrum was taken from 5 to 120 degrees of Bragg angles, focusing the goniometer according to the Bragg–Brentano scheme. The expert's work is based on the use of software for testing directives: X'expert High Score Plus version 2.2b and X'expert High Score version 2.2b.

## 3. Results

Table 2 shows the chemical composition of the obtained samples.

**Table 2.** The composition of the alloys.

| Smp/Elem, % | Co | Cr | Fe | Ni | Mn | Nb | C | Si | P | S |
|---|---|---|---|---|---|---|---|---|---|---|
| 1 | 16.94 | 16.82 | 18.5 | 16.73 | 16.53 | 14.23 | 0.23 | 0.002 | trace | trace |
| 2 | 16.78 | 16.54 | 17.88 | 16.72 | 16.28 | 15.51 | 0.25 | 0.002 | trace | trace |
| 3 | 16.58 | 16.60 | 17.54 | 16.34 | 16.32 | 16.33 | 0.28 | 0.002 | trace | trace |
| 4 | 16.89 | 16.65 | 15.42 | 16.67 | 16.82 | 17.22 | 0.32 | 0.0022 | trace | trace |
| 5 | 16.67 | 16.86 | 14.60 | 16.49 | 16.60 | 18.45 | 0.32 | 0.0022 | trace | trace |

The sufficiently high C content in the experimental alloys is explained by the fact that the melting was carried out in a graphite crucible and in an air atmosphere; therefore, a carburization process took place. In addition, ferroalloys are not two-component systems as they contain impurities such as C, Si, S, and P. Niobium is a strong carbide-forming agent; therefore, it is logical to assume that niobium carbides are formed during crystallization. Carbides are solid phases, and their presence will certainly have a significant impact on the hardness and wear resistance of the alloy.

It is seen from the data in Table 2 that the iron content in some experimental alloys (samples 1–3) is slightly higher than the content of the other elements, which is understandable, because iron is included in the three components of the charge. However, all of the alloys under study comply with the "high entropy" principle, and none of the alloy elements is a base element.

Figure 2 shows the structure of the experimental alloy (sample 2). The matrix of the structure is represented by a solid solution that includes Fe, Co, Cr, Mn, Ni, and Nb. In general, at least three phases can be distinguished in the structure: an interstitial phase and solid solutions of various compositions. Phases containing elements with higher

atomic numbers in the structure obtained in the BSD mode appear lighter, so it is logical to assume that the structure contains phases with different contents of niobium as the heaviest element: those with a higher content of niobium and those depleted in niobium. A similar picture was observed in work [11], where two solid solutions with different molybdenum contents were recorded. In the same work, it was noted that increasing the niobium content above 1.2% wt. led to increasing the amount of Laves phase. In addition to the solid solution, this structure also contains interstitial phases, possibly carbide, given the presence of carbon in the alloy.

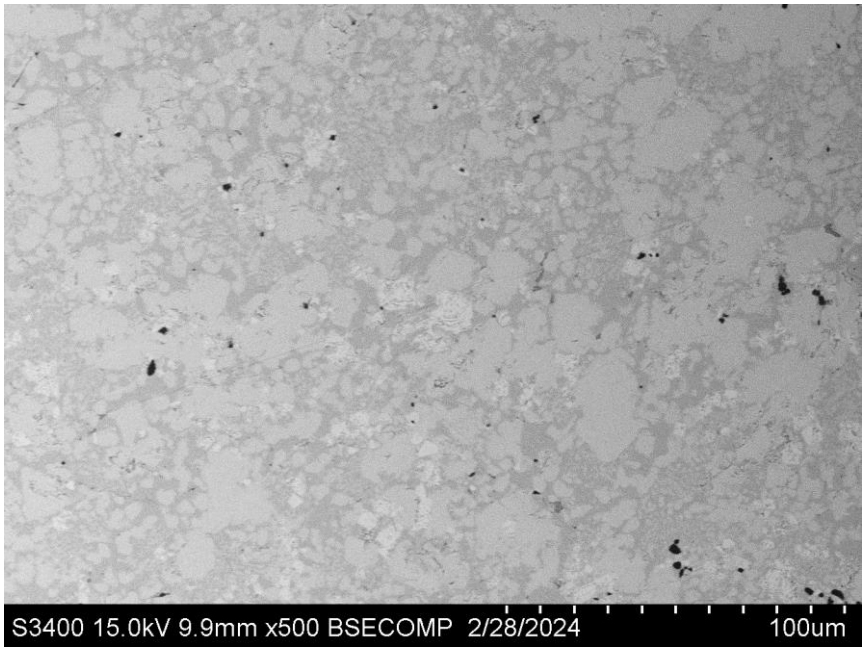


**Figure 2.** The experimental alloy structure (sample 2).

It should be noted that this structure is typical for all of the studied samples, with the exception of sample 5, for which there are areas characterized by a high niobium content, confirmed by the element distribution map (Figure 3). Though all of the components of the alloy are distributed relatively evenly, the distribution of Nb is clearly non-uniform.

This fact occurs when the Nb content in the sample is more than 18%. The uneven distribution of Nb in the solid solution can most likely be explained by the decrease in the diffusion coefficient of the element that is caused by a significantly greater distortion of the solid solution lattice at this Nb content level.

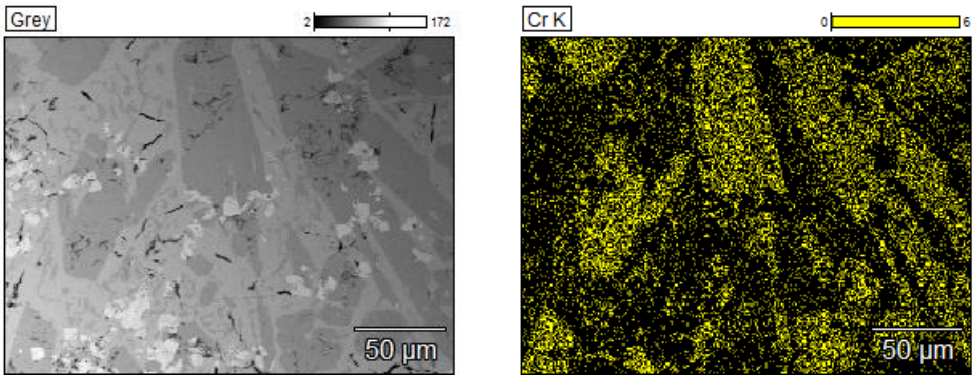

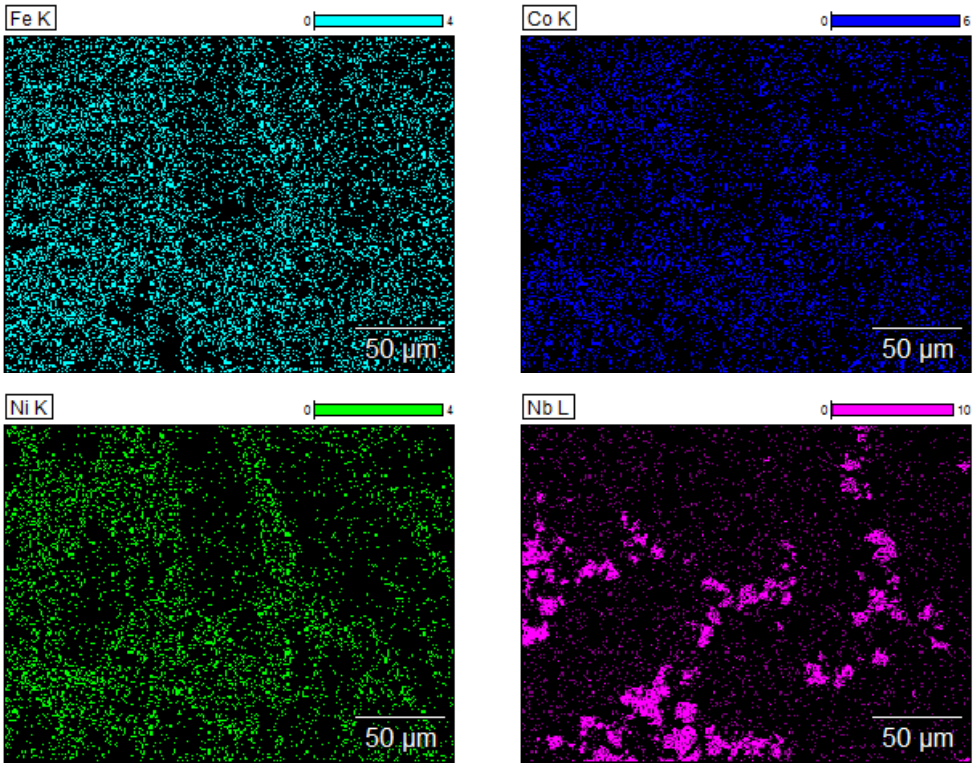


**Figure 3.** Map of element distribution in sample 5.

It should be noted that according to the MXSA data, the presence of silicon, oxygen, and carbon is observed; however, carbon was not noted at the studied points, and oxygen and silicon were only noted in some fields (Figure 4). The presence of silicon, oxygen, and carbon in the samples is explained by their presence in the charge, the melting in the open air, and the development of the carburization process, since melting was carried out in a graphite crucible.

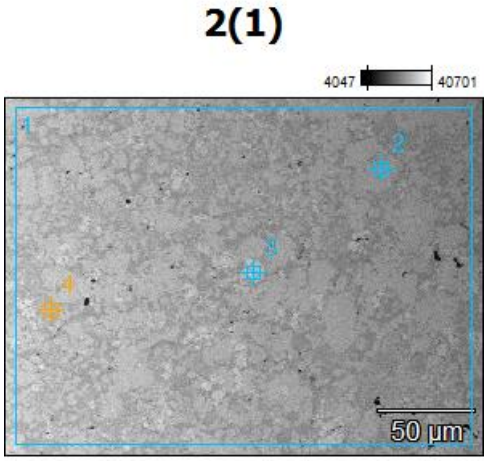

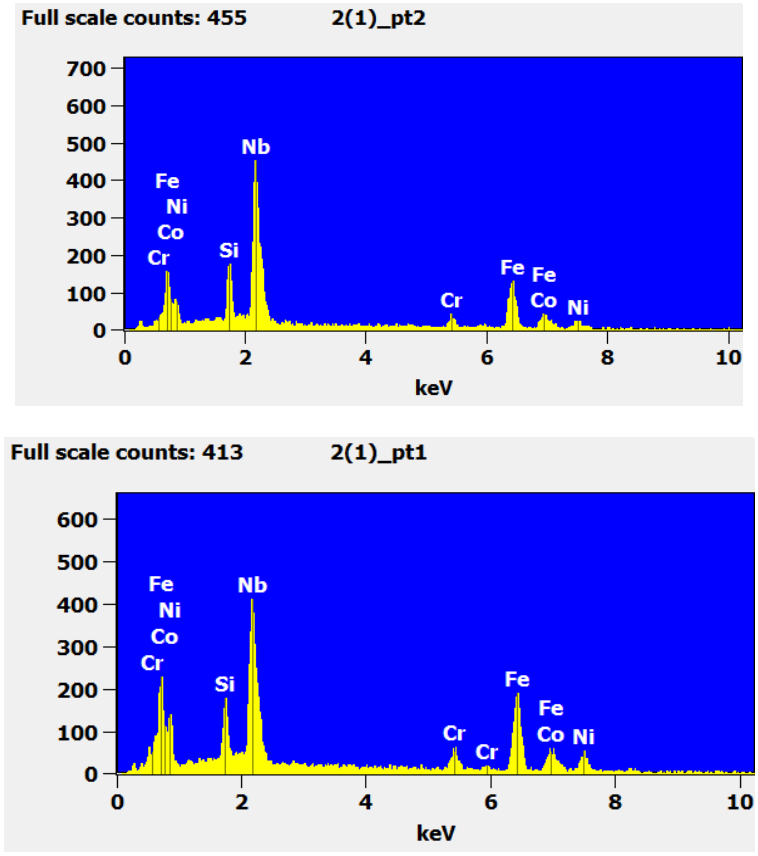


**Figure 4.** MXSA results for sample 2.

The results shown in Table 3 demonstrate the presence of solid solutions in the structure with different niobium contents (points 1, 2, 4). At point 3, the niobium content is 96.8% and the rest is oxygen. Niobium oxide is present at point 1. There is no carbon at any of the studied points. However, given its presence in the alloy (Table 2), it is logical to assume the presence of a carbide phase, possibly niobium carbides and carbides of the M7C3 or cementite type.

**Table 3.** MXSA results for sample 2.

| | O-K | Si-K | Cr-K | Fe-K | Co-K | Ni-K | Nb-L |
|---|---|---|---|---|---|---|---|
| 2(1)_pt1 | | 4.2 | 5.9 | 37.8 | 9.1 | 14.9 | 28.2 |
| 2(1)_pt2 | | 6.1 | 3.8 | 33.0 | 8.9 | 9.1 | 39.0 |
| 2(1)_pt3 | 3.2 | | | | | | 96.8 |
| 2(1)_pt4 | | 3.1 | 8.6 | 50.3 | 10.5 | 19.8 | 7.7 |

At this stage of the study, the presence of the Laves phase that is mentioned in works [19–24] was not observed. It should be noted that there is some discrepancy between the MXSA data and the composition of the alloy according to the spectrometry data. It is obvious that this is caused by the segregation of the composition and non-uniform distribution of the elements.

In order to identify the phases in which these elements are present, an X-ray phase analysis (XFA) was performed, the results of which are shown in Figure 5.

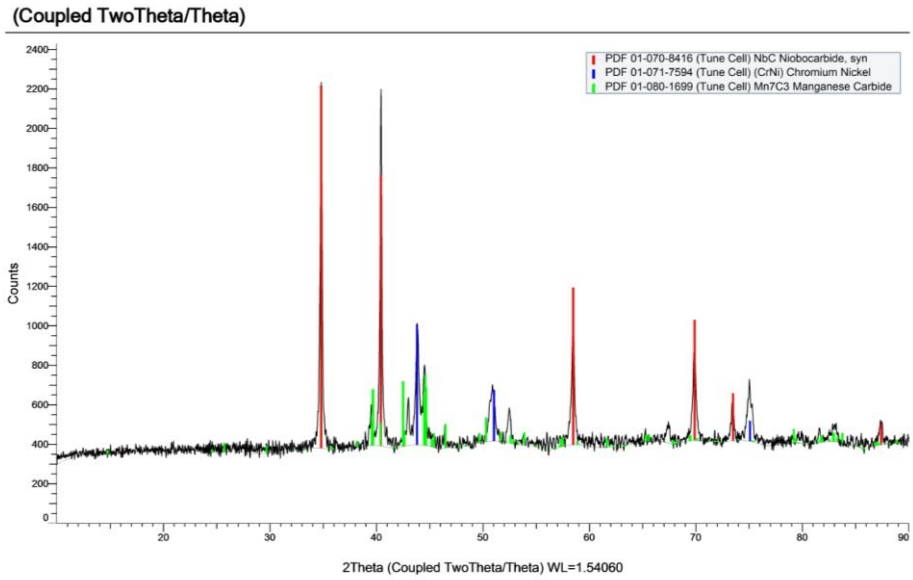


Sample 2

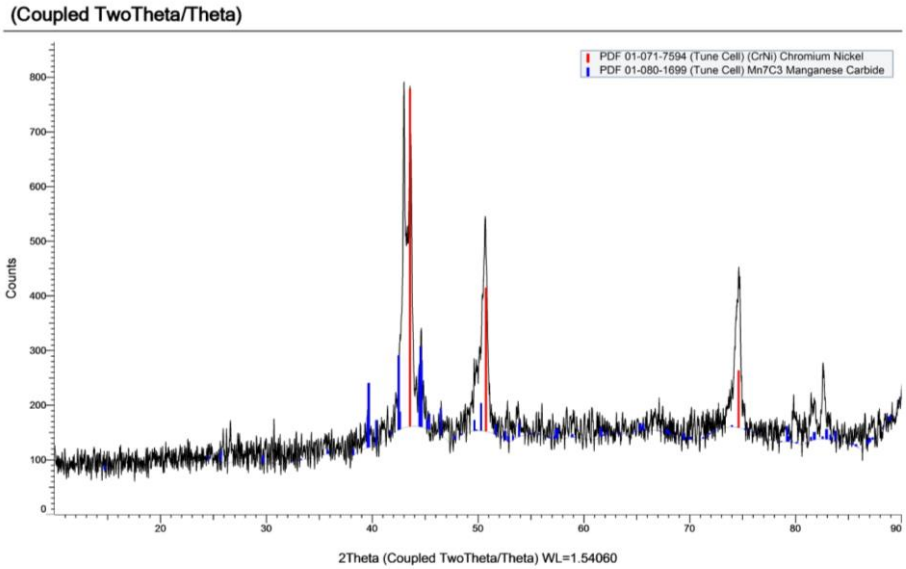


Sample 3

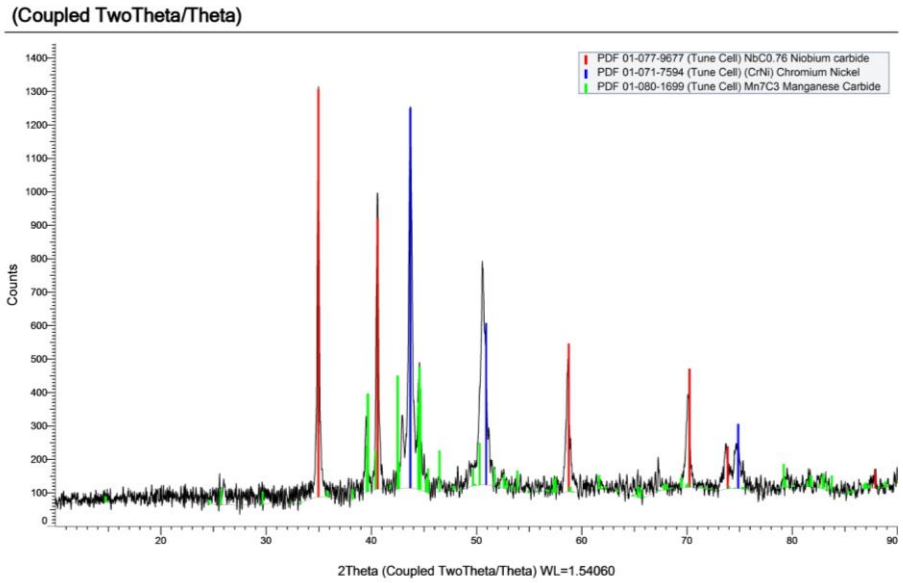


Sample 5

**Figure 5.** XRD results for experimental samples with different niobium content.

The XRD results show that all samples contain an FCC solid solution in which all metals are dissolved, as well as niobium carbide type NbC0.76–1.0, manganese carbide type $Mn_7C_3$, and intermetallic-type CrNi with a cubic lattice. It was not possible to determine in which phases silicon is present in this study, although MXSA and general chemical analysis show its presence. It is possible that silicon is part of the BCC solution, the presence of which is assumed according to thermodynamic calculations and is noted in [1,6,22]. However, these peaks were not recorded on radiographs, which may be due to the low content of BCC in the sample.

It should be noted that the results obtained differ somewhat from the data obtained in [20,21,24], which note the presence of eutectic consisting of a solid solution and a Laves phase. The discrepancy is perhaps due to the difference in the charge and the presence of additional elements such as oxygen, silicon, and carbon and the melting and crystallization conditions under which this phase formation mechanism is not realized.

As can be seen from the data in Table 3, sample 2 (with a total niobium content of 15.5% by weight) shows a very large variation in niobium content at different points. In points 1 and 2, according to the XRF data, there is an FCC solid solution with a different niobium content. An analysis of the data in Table 3 suggests that the solubility of niobium in solution reaches 39%.

There is also a significant amount of silicon in these areas, apparently part of the solid solution, because it is not released into a separate phase. Point 3, judging by the high content of niobium and oxygen, reflects a non-metallic inclusion of the oxide type. Point 4 is an iron-based solid solution, and the presence of manganese at this point is not observed.

Sample 5 (niobium content 18.45%, Table 2) is also represented by a solid solution with different niobium content: depleted (dark areas) or, vice versa, overenriched with niobium (light gray areas).

Strength and hardness tests were carried out on prototypes, and tribological characteristics were determined. All tests were carried out in triplicate to confirm their reliability. Table 4 presents the results obtained. The pure Cantor alloy (CoCrFeMnNi) was used as the comparison sample.

**Table 4.** Results of the tests carried out.

| Sample | Hardness, HV | Compression Strength, MPa | Unit Shortening, % | Friction Coefficient | Wear Bandwidth, μm | Sample Reduced Wear, $mm^3/(N \cdot m)$ |
|---|---|---|---|---|---|---|
| Cantor alloy | 240 | 550 | 28.51 | 0.45 | 172.2 | $3.67 \times 10^{-6}$ |
| 1 | 243 | 550 | 21.24 | 0.44 | 167.4 | $3.24 \times 10^{-6}$ |
| 2 | 282 | 630 | 17.45 | 0.42 | 146.8 | $2.92 \times 10^{-6}$ |
| 3 | 395 | 720 | 15.69 | 0.39 | 145.4 | $1.88 \times 10^{-6}$ |
| 4 | 446 | 725 | 14.28 | 0.37 | 144.9 | $1.75 \times 10^{-6}$ |
| 5 | 367 | 632 | 14.40 | 0.43 | 178.3 | $3.04 \times 10^{-6}$ |

The data in Table 4 show that, in general, the presence of niobium in the alloy has a positive effect on the strength properties and wear resistance. These properties increase with a niobium content of up to 16.85% (sample 4). When the niobium content in the sample surpasses 18% (sample 5), the hardness remains virtually unchanged, but its strength, coefficient of friction, and wear resistance deteriorate. This tendency is probably associated with the inhomogeneity of the surface structure caused by the uneven distribution of niobium.

Figure 6 shows photos of wear tracks on samples 2 and 5. The unetched structures of the samples after ultrasonic cleaning are presented; the size of the samples must be at least 10 mm in at least one dimension and not exceed the dimensions of the holder (Figure 6).

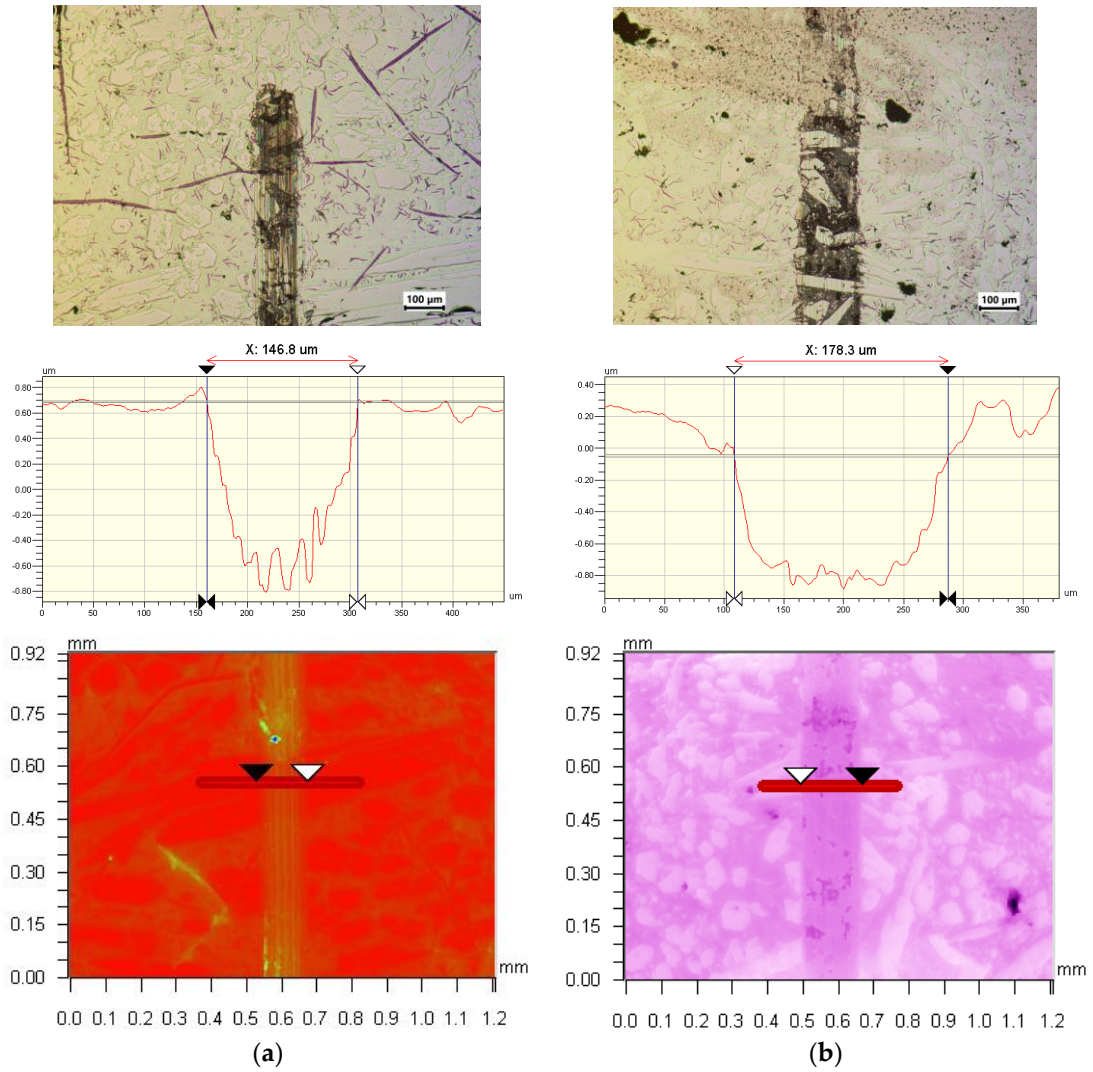


**Figure 6** Photos of wear tracks on experimental samples: (**a**), sample 2; (**b**), sample 5.

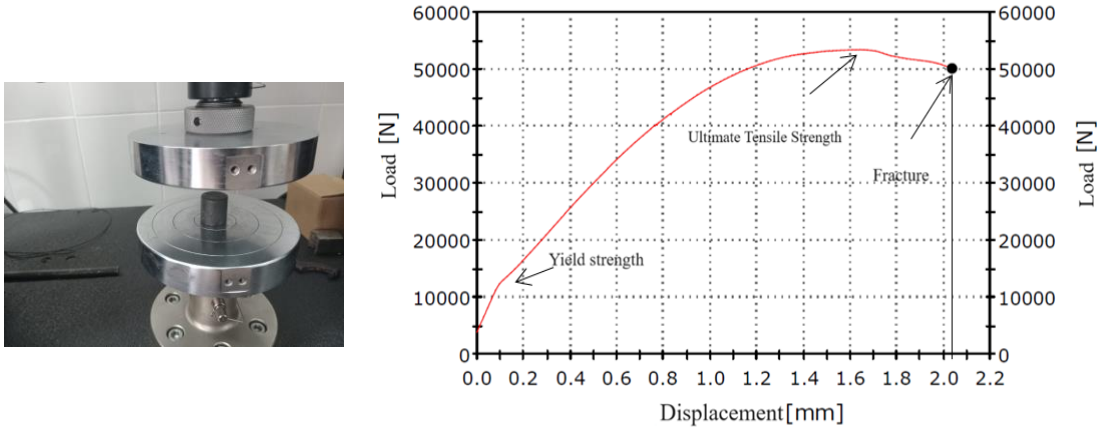


**Figure 6.** Sample 2—compression test.

A visual comparison of the width and intensity of the wear tracks shows that sample 5 has less wear resistance than sample 2, which is consistent with the data shown in Table 2.

Figure 5 shows a characteristic pattern of abrasive wear. There are zones of plastic deformation along the furrow, which is a typical feature of abrasive wear [29–33].

Using the setup, a standard curve was obtained, from which it is possible to determine the main strength characteristics of the sample behavior under compression: yield strength, ultimate strength, point of formation of a sample fracture.

Figure 6 shows an example of the compression tests, and the results are shown in Table 4.

The studies have shown that initially, when the sample is compressed, like most metal samples, it acquires a barrel-like shape due to the occurrence of a friction force on the end surfaces of the sample. With further compression, the formation of a crack and further destruction occurs along the direction of the load on the sample (Figure 7). This indicates fracture by separation that in turn indicates brittle fracture that occurs from the presence of interstitial phases and due to not very high ductility of the material. At the same time, please note that the studies carried out comprise the initial stage of the research and are designed to show the fundamental possibility of using not pure metals but ferroalloys in the charge to produce QHEAs. At the same time, a new area of studies arises: increasing plasticity by introducing new elements.

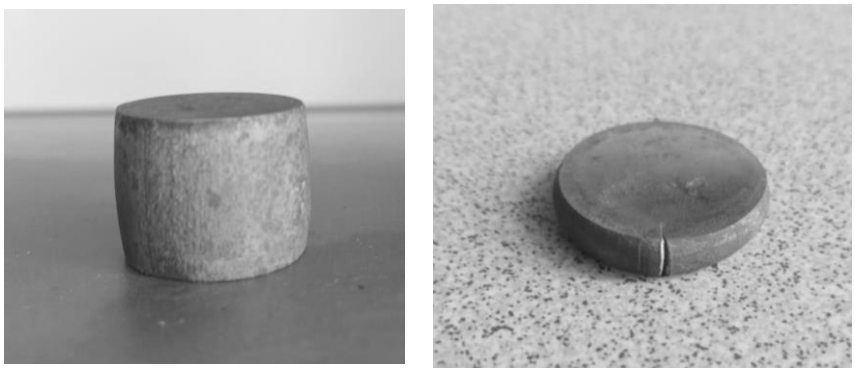

(**a**) (**b**)

**Figure 7.** (**a**) The barrel-like shape of the sample after a violation of the uniformity of deformation; (**b**) A sample crack under compression.

According to [20,21,23,24], plasticity decreases with an increase in the niobium content, which is in good agreement with the results obtained for the experimental samples (Table 4). In the absence of niobium in the alloy, the plasticity is 28.51%; in sample 2 (ni-

obium content of 15.5%), it is 17.45%, and further, a decrease in plasticity is observed with an increase in the niobium content. The authors in [20,21,23,24] attribute this trend to an increase in the content of the Laves phase. In this study, this trend can be explained by an increase in the content of niobium carbide in the structure.

As can be seen from the data in Table 5, the niobium content in the alloy has a significant effect on all of the properties under study. The hardness, compressive strength, and wear resistance increase with an increase in the niobium content, with the exception of a sample with a niobium content of more than 18%.

**Table 5.** Casting properties of the samples studied.

| Sample | Fluidity, % | Fillability, % | | | | Linear Shrinkage, % |
|---|---|---|---|---|---|---|
| | | Ø 5 | Ø 10 | Ø 15 | Ø 20 | |
| Cantor alloy (standard) | 26 | 70 | 90 | 95 | 100 | 2.1 |
| 1 | 24 | 50 | 75 | 90 | 100 | 1.9 |
| 2 | 23 | 45 | 70 | 88 | 100 | 1.8 |
| 3 | 18 | 45 | 67 | 85 | 100 | 1.8 |
| 4 | 17 | 40 | 60 | 85 | 100 | 1.7 |
| 5 | 15 | 35 | 57 | 82 | 100 | 1.7 |

In this alloy, all strength properties and wear resistance decrease and become comparable to the values of the sample without niobium. The decrease in these properties can be associated with an extremely heterogeneous distribution of niobium, as evidenced by the maps of the distribution of elements (Figure 3). The pronounced segregation of niobium along the boundaries in sample 5 leads to the formation of additional stress sources, which leads to the possible crumbling of surface nanoparticles and an increase in the wear furrow.

The authors in [20,21,24] associate an increase in strength, hardness, and wear resistance with the formation of a solid and durable Laves phase and note a proportional relationship between the content of the Laves phase in the structure and strength properties.

However, in this study, the presence of the Laves phase was not noted in the experimental alloys, while phases of incorporation such as niobium carbide and manganese carbide were observed in the structure.

These phases of implementation also have high hardness and strength. Their presence in the relatively plastic matrix of the FCC solution corresponds to the optimal structure of wear-resistant materials according to the Sharpie principle: a matrix with a uniformly distributed and highly dispersed solid phase of implementation.

To increase the commercial attractiveness of QHEAs and their further use as casting alloys, it is also necessary to consider their casting properties. For this purpose, technological properties of experimental QHEAs such as fluidity, mold fillability, and linear shrinkage were considered.

The fillability of the molds was determined using samples in the shape of a cylindrical rod 200 mm long, with four outlet channels with different diameters from 5 mm to 20 mm and the length of 100 mm.

Fluidity was determined according to SS 16438-70 [34].

Initially, the model was made of a paraffin–stearin mixture in the ratio of 50:50. The paraffin–stearin mixture, heated to 50–60 °C, was poured into a detachable metal mold, the cavity of which was a rod 200 mm long and 30 mm in diameter. After cooling and hardening, the model was removed from the mold and controlled using calipers to measure the geometric dimensions. Next, the shell was created. To execute this, the resulting model was immersed in a refractory mixture consisting of quartz sand of two main fractions, 0.16 mm and 0.05 mm, mixed with a clay suspension. After removal from

the refractory mixture, the shell was dried in a stream of air for 20 min. The model was removed by heating it with boiling water and subsequently draining the paraffin–stearin mixture from the shell. After this operation, to remove moisture, the shell was dried at a temperature of 80 °C for 12 h. The next stage was its calcination. For this process, the shell was placed in a Nabertherm oven, heated to a temperature of 700 °C over 30 min, and kept at this temperature for about 20 min to completely gasify the remains of the model composition. After cooling to the ambient temperature, the shell mold was ready for pouring. This method of producing castings is a precision method that ensures high geometric and dimensional accuracy. The liquid metal poured into the shell filled the cavity of the specified dimensions.

In this case, the cooling melt had free shrinkage both along the sample length and diameter. After cooling, the sample was removed from the mold, and the diameter and length were measured. After hardening, the sample had smaller dimensions due to shrinkage.

Using the models, molds are made to obtain samples. Models have holes with a distance of 200 mm between them. Before removing the models from the molds, conical recesses are made on the mold through the holes using a metal core. After pouring and cooling the casting, there is used a caliper to measure the distance between the protrusions on the casting $l_{cast}$. Shrinkage is determined by means of comparing the distance between the centers of conical depressions in the mold and between the corresponding protrusions on the casting. Free shrinkage is determined using a sample, the drawing of which is presented in Figure 8.

The linear shrinkage of melts was assessed using special samples produced by investment casting (Figure 9).

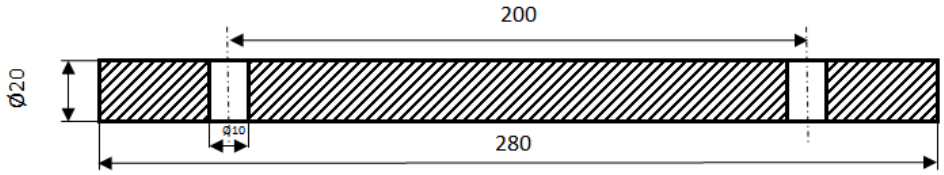


**Figure 8.** Drawing of samples for determining free shrinkage.

The amount of linear shrinkage is determined by the formula:

$$\varepsilon_{lin} = \frac{200 - l_{cast}}{l_{cast}} \times 100\%.$$

**Figure 9.** A mold for obtaining special samples for determining linear shrinkage.

The results of studying the casting properties are presented in Table 5.

The data in Table 5 show that the presence of niobium in the amount of 14–16% (samples 1–3) has virtually no effect on the melt fluidity; however, increasing the niobium content in the alloy over 17% (samples 4–5) significantly reduces the melt fluidity, which is obviously associated, as noted above, with the uneven distribution of niobium throughout the volume of the melt and, in particular, its increased content in the frontal part of the melt flow.

The presence of niobium, regardless of its content, reduces the fillability of narrow channels with a diameter of 10 mm or less.

From the point of view of linear shrinkage, the presence of niobium in the Cantor alloy contributes to its reduction throughout the entire concentration range studied.

It should be expected that the partial use of ferroalloys instead of pure metals will reduce the cost of the alloy. For this purpose, the cost of an alloy made from pure metals and an experimental alloy made using ferromanganese and ferrochrome was calculated; only the cost of the charge materials per 1 kg was taken into account. The calculation was carried out in conventional units because the real cost depends on the region and many other factors. Nevertheless, this calculation provided an indication of the possible costs saved from the partial use of ferroalloys in the charge instead of pure metals.

An approximate calculation (Table 6) shows that the cost of the charge for smelting one kilogram of an alloy of pure metals is approximately 44.5 CU; for an experimental alloy obtained using ferroalloys, this value is 21.8 y.e.

**Table 6.** Calculation of the cost of the charge.

| Component | Weight per 1 kg | Cost of the Components for the Charge When Smelting an Alloy of Pure Metals | Cost of the Components for the Charge When Smelting an Experimental Alloy Using Ferroalloys |
|---|---|---|---|
| Ferromanganese FeMn80C05 | 235 g | - | 1.6 |
| Ferrochrome FH70 | 324 g | - | 2.1 |
| Ferroniobium FNb65 | 378 g | - | 7.8 |
| Ni H-1y Nickel | 178 g | 3.1 | 3.1 |
| Cobalt Co K1Ay | 161 g | 7.2 | 7.2 |
| Chrome X99H1 | 227 g | 2.0 | - |
| Manganese Mn998 | 188 g | 3.1 | - |
| Niobium Nb-1 | 246 g | 19.1 | - |
| Total: | | 34.5 y.e. | 21.8 y.e. |

Thus, due to the charge materials, savings of more than 40% can be achieved provided that all other melting parameters remain the same. With the conditional serial production of 100,000 parts weighing 0.3 kg per year, the cost savings will amount to approximately 0.38 million y.e.

## 4. Conclusions

The studies carried out involved the partial replacement of pure metals with ferroalloys of an appropriate nature when smelting QHEAs. A correctly selected charge makes it possible to obtain an alloy similar in composition and properties to QHEAs that are smelted using pure metals.

The introduction of niobium in the amount of 14–17% into the Cantor alloy leads to significant increases in the hardness, strength, and wear resistance of the alloy. A niobium content of more than 18% in an alloy based on the CoCrFeMnNi system is undesirable, because it leads to the non-uniform distribution of niobium in the solid solution, which is associated with a decrease in the diffusion coefficient.

The structure of the studied alloys is represented by a solid solution of FCC, which includes all metals, and the niobium content varies widely. In addition, the structure is represented by the phases of implementation: niobium carbide NbC 0.76–1.0, manganese carbide $Mn_7C_3$, and a CrNi intermetallic compound with a cubic lattice.

The non-uniform distribution of niobium decreases the strength and wear resistance of the sample and also reduces technological casting properties such as fluidity and mold fillability.

**Author Contributions:** S.K. and A.I. conceived and designed the concept of the research and methodology. V.K. and S.A. performed material investigations and contributed to the paper's editing. S.A. performed metallographic studies, further data analysis, and interpretation. S.K., A.I., and V.K. supervised and substantively revised all work and the article text. All authors participated in writing the paper. All authors have read and agreed to the published version of the manuscript.

**Funding:** This research was funded by the Science Committee of the Ministry of Science and Higher Education of the Republic of Kazakhstan (Grant No. BR21882240): "Developing a quasi-high-entropy alloy using Kazakhstan raw materials and the technology of producing precision parts based on it".

**Institutional Review Board Statement:** Not applicable.

**Informed Consent Statement:** Not applicable.

**Data Availability Statement:** The raw data supporting the conclusions of this article will be made available by the authors on request.

**Conflicts of Interest:** The authors declare no conflicts of interest.

## References

1. Cantor, B.; Chang, I.T.H.; Knight, P.; Vincent, A.J.B. Microstructural development in equiatomic multicomponent alloys. *Mater. Sci. Eng. A* **2004**, *375–377*, 213–218. https://doi.org/10.1016/j.msea.2003.10.257.
2. Yeh, J.-W. Recent Progress in High Entropy Alloys. *Ann. Chim. Sci. Mat.* **2006**, *31*, 633–648. https://doi.org/10.3166/acsm.31.633-648.
3. Miracle, D.B.; Senkov, O.N.; Wilks, J. A critical review of high entropy alloys and related concepts. *Acta Mater.* **2017**, *122*, 448–511. https://doi.org/10.1016/j.actamat.2016.08.081.
4. Ranganathan, S. Alloyed pleasures: Multimetallic cocktails. *Curr. Sci.* **2003**, *85*, 1404–1406.
5. Li, D.; Liaw, P.K.; Xie, L.; Zhang, Y.; Wang, W. Advanced high-entropy alloys breaking the property limits of current materials. *J. Mater. Sci. Technol.* **2024**, *186*, 219–230. https://doi.org/10.1016/j.jmst.2023.12.006.
6. Yeh, J.W.; Chen, Y.L.; Lin, S.J.; Chen, S.K. High-entropy alloys—a new era of exploitation. *Mater. Sci. Forum* **2007**, *560*, 1–9. https://doi.org/10.4028/www.scientific.net/msf.560.1.
7. Cantor, B. Multicomponent high-entropy Cantor alloys. *Prog. Mater. Sci.* **2021**, *120*, 100754. https://doi.org/10.1016/j.pmatsci.2020.100754.
8. Takeuchi, A.; Amiya, K.; Wada, T.; Yubuta, K.; Zhang, W. High-entropy alloys with a hexagonal close-packed structure designed by equi-atomic alloy strategy and binary phase diagrams. *JOM* **2014**, *66*, 1984–1992. https://doi.org/10.1007/s11837-014-1085-x.
9. Zhang, Y.; Zuo, T.T.; Tang, Z.; Gao, M.C.; Dahmen, K.A.; Liaw, P.K.; Lu, Z.P. Microstructures and properties of high-entropy alloys. *Prog. Mater. Sci.* **2014**, *61*, 1–93.
10. Gali, A.; George, E. Tensile properties of high- and medium-entropy alloys. *Intermetallics* **2013**, *39*, 74–78. https://doi.org/10.1016/j.intermet.2013.03.018.
11. Sathiyamoorthi, P.; Kim, H.S. High-entropy alloys with heterogeneous microstructure: Processing and mechanical properties. *Prog. Mater. Sci.* **2022**, *123*, 100709. https://doi.org/10.1016/j.pmatsci.2020.100709.
12. Chen, Y.; Liu, W.; Wang, H.; Xie, J.; Zhang, T.; Yin, L.; Huang, Y. Effect of Ti Content on the Microstructure and Properties of CoCrFeNiMnTix High Entropy Alloy. *Entropy* **2022**, *24*, 241. https://doi.org/10.3390/e24020241.
13. Lin, C.-M.; Tsai, H.-L. Effect of annealing treatment on microstructure and properties of high-entropy FeCoNiCrCu0.5 alloy. *Mater. Chem. Phys.* **2011**, *128*, 50–56. https://doi.org/10.1016/j.matchemphys.2011.02.022.
14. Tong, C.-J.; Chen, M.-R.; Yeh, J.-W.; Lin, S.-J.; Chen, S.-K.; Shun, T.-T.; Chang, S.-Y. Mechanical performance of the $Al_x$-CoCrCuFeNi high-entropy alloy system with multiprincipal elements. *Met. Mater. Trans. A* **2005**, *36*, 1263–1271. https://doi.org/10.1007/s11661-005-0218-9.
15. Zhang, Y.; Yang, X.; Liaw, P.K. Alloy design and properties optimization of high-entropy alloys. *JOM* **2012**, *64*, 830–838. https://doi.org/10.1007/s11837-012-0366-5.

16. Ma, X.; Chen, J.; Wang, X.; Xu, Y.; Xue, Y. Microstructure and mechanical properties of cold drawing CoCrFeMnNi high entropy alloy. *J. Alloy. Compd.* **2019**, *795*, 45–53. https://doi.org/10.1016/j.jallcom.2019.04.296.
17. Bazlov, A.; Strochko, I.; Ubyivovk, E.; Parkhomenko, M.; Magomedova, D.; Zanaeva, E. Structure and Properties of Amorphous Quasi-High-Entropy Fe-Co-Ni-Cr-(Mo,V)-B Alloys with Various Boron Content. *Metals* **2023**, *13*, 1464. https://doi.org/10.3390/met13081464.
18. Gludovatz, B.; George, E.P.; Ritchie, R.O. Processing, Microstructure and Mechanical Properties of the CrMnFeCoNi High-Entropy Alloy. *JOM* **2015**, *67*, 2262–2270. https://doi.org/10.1007/s11837-015-1589-z.
19. Salishchev, G.; Tikhonovsky, M.; Shaysultanov, D.; Stepanov, N.; Kuznetsov, A.; Kolodiy, I.; Tortika, A.; Senkov, O. Effect of Mn and V on structure and mechanical properties of high-entropy alloys based on CoCrFeNi system. *J. Alloy. Compd.* **2014**, *591*, 11–21. https://doi.org/10.1016/j.jallcom.2013.12.210.
20. Zhang, J.; Xiong, K.; Huang, L.; Xie, B.; Ren, D.; Tang, C.; Feng, W. Effect of Doping with Different Nb Contents on the Properties of CoCrFeNi High-Entropy Alloys. *Materials* **2023**, *16*, 6407. https://doi.org/10.3390/ma16196407.
21. Jiang, H.; Jiang, L.; Qiao, D.; Lu, Y.; Wang, T.; Cao, Z.; Li, T. Effect of Niobium on Microstructure and Properties of the CoCrFeNbxNi High Entropy Alloys. *J. Mater. Sci. Technol.* **2017**, *33*, 712–717. https://doi.org/10.1016/j.jmst.2016.09.016.
22. He, F.; Wang, Z.; Wu, Q.; Li, J.; Wang, J.; Liu, C. Phase separation of metastable CoCrFeNi high entropy alloy at intermediate temperatures. *Scr. Mater.* **2017**, *126*, 15–19. https://doi.org/10.1016/j.scriptamat.2016.08.008.
23. Huang, S.; Wu, H.; Zhu, H.; Xie, Z. Effect of niobium addition upon microstructure and tensile properties of CrMnFeCoNi$_x$C high entropy alloys. *Mater. Sci. Eng. A* **2021**, *809*, 140959. https://doi.org/10.1016/j.msea.2021.140959.
24. Zhang, H.; Wang, H.; Liu, Y. Improved strength and ductility in a Co-Cr-Fe-Ni-Mo high-entropy alloy system. *J. Alloys Compd.* **2014**, *586*, 478–483.
25. Gogebakan, M.; Kursun, C.; Gunduz, K.O.; Tarakci, M.; Gencer, Y. Microstructural And Mechanical Properties Of Binary Ni-Si Eutectic Alloys. *J. Alloy. Compd.* **2015**, *643*, S219–S225. https://doi.org/10.1016/j.jallcom.2014.12.058.
26. *ASTM G99-05*; Standard Test Method for Wear Testing with a Pin-on-Disk Apparatus. ASTM: West Conshohocken, PA, USA, 2010.
27. *ASTM G133-05*; Standard Test Method for Linearly Reciprocating Ball-on-Flat Sliding Wear. ASTM: West Conshohocken, PA, USA, 2010.
28. DIN 50324:1992-07; Tribology; Testing of Friction and Wear Model Test for Sliding Friction of Solids (Ball on Disc System). German Institute for Standardisation: Berlin, Germany, 1992.
29. Yang, L.; Li, Y.; Wang, Z.; Zhao, W.; Qin, C. Nanoporous Quasi-High-Entropy Alloy Microspheres. *Metals* **2019**, *9*, 345. https://doi.org/10.3390/met9030345.
30. Zeng, Z.; Xiang, M.; Zhang, D.; Shi, J.; Wang, W.; Tang, X.; Tang, W.; Wang, Y.; Ma, X.; Chen, Z.; et al. Mechanical properties of Cantor alloys driven by additional elements: A review. *J. Mater. Res. Technol.* **2021**, *15*, 1920–1934. https://doi.org/10.1016/j.jmrt.2021.09.019.
31. Wu, H.; Zhang, S.; Wang, R.; Zhang, H.; Zhang, C.; Wu, C.; Chen, H. Exploration of wear and slurry erosion mechanisms of laser clad CoCrFeNi + x (NbC) high entropy alloys composite coatings. *Tribol. Int.* **2024**, *193*, 109405. https://doi.org/10.1016/j.triboint.2024.109405.
32. Wang, Y.; Yang, Y.; Yang, H.; Zhang, M.; Ma, S.; Qiao, J. Microstructure and wear properties of nitrided AlCoCrFeNi high-entropy alloy. *Mater. Chem. Phys.* **2018**, *210*, 233–239. https://doi.org/10.1016/j.matchemphys.2017.05.029.
33. Du, L.; Lan, L.; Zhu, S.; Yang, H.; Shi, X.; Liaw, P.; Qiao, J. Effects of temperature on the tribological behavior of $Al_{0.25}$CoCrFeNi high-entropy alloy. *J. Mater. Sci. Technol.* **2019**, *35*, 917–925. https://doi.org/10.1016/j.jmst.2018.11.023.
34. *GOST (State Standard) 16438–70*; Sand and Metallic Molds for Obtaining the Samples of Fluidity of Metals. Izd. Standartov: Moscow, Russia, 1999.